Supplementary Materials

In situ growth of B, N-doped Fe_3C-encapsulated carbon nanotubes on wood-derived carbon for high-performance Zn-air battery electrocatalysts

Ming Li, Wenhui Zhu, Chen Wang, Jialin Fan, Yongzhuang Liu, Qinqin Xia, Haipeng Yu, Shuo Dou*

Key Laboratory of Bio-based Material Science and Technology of Ministry of Education, Northeast Forestry University, Harbin 150040, Heilongjiang, China.

***Correspondence to:** Prof. Shuo Dou, Key Laboratory of Bio-based Material Science and Technology of Ministry of Education, Northeast Forestry University, Harbin 150040, Heilongjiang, China. E-mail: doushuo@nefu.edu.cn

1. Chemicals and materials

The balsa wood used in this study was sourced from Ecuador in South America. Acetic acid, sodium acetate, sodium chlorite (80%), melamine, urea, boric acid, anhydrous ferric chloride, potassium hydroxide, and zinc acetate were all obtained from Aladdin Co., Ltd. Hydrochloric acid was purchased from Foshan XiLong Chemical Co., Ltd. platinum on carbon (20 wt% loading) was procured from Beijing Inno-chem Technology Co., Ltd. Ruthenium oxide (Ru≥75 wt%) was procured from Suzhou Sinero Technology Co., Ltd. Unless otherwise stated, all chemicals were of analytical grade and were used without any additional purification. Ultrapure water was used throughout the experiment.

2. Lignin content analysis

The compositions of the lignin were determined according to the NREL procedure[1]. Briefly, 0.3 g of oven-dried sample was placed in a screw-capped glass bottle, and 3 mL of 72 wt% sulfuric acid was added. The mixture was manually stirred with a glass rod at room temperature using alternating 10 min stirring at approximately 50 rpm and 10 min standing intervals, until a cumulative stirring time of 1 h was reached. The mixture was then diluted to a sulfuric acid concentration of 3 wt% and heated at 121 °C for 1 h. After cooling to room temperature, the undissolved solid was filtered and dried to determine the lignin content. Acid insoluble lignin was used to calculate the lignin content in the original lignocellulose.

3. Characterization

The sample morphology was characterized using a scanning electron microscope (SEM, SUPRA 55, Carl Zeiss Microscopy GmbH, Germany) and a high-resolution transmission electron microscope (HRTEM, JEM-F200, JEOL Ltd., Japan). Raman measurements were carried out using a Raman spectrometer (LabRAM HR Evolution, HORIBA France SAS, France). Powder XRD was conducted in the 2θ range of 5~80° with Cu Kα radiation (X'Pert PRO, PANalytical B.V., The Netherlands). XPS was performed on a Thermo electron spectrometer (XPS, K-Alpha, Thermo Fisher Scientific, UK) to investigate the bonding characteristics. The specific surface area of samples was measured by the Brunauer–Emmett–Teller (BET) method based on N_2 adsorption/desorption isotherms, which were performed at 77 K using an automated adsorption apparatus (BET, ASAP 2460, Micromeritics Instrument Corporation, USA). The electrical conductivity was tested using an RTS-8 digital four-probe tester (RTS-8, Guangzhou Four Probe Technology Co., Ltd., China). Discs with a diameter of 10 mm were prepared. The thickness of each disc was measured using a thickness gauge with an accuracy of 0.001 mm. For each sample, five measurements were taken on both the front and back sides of the discs.

4. Electrochemical measurements

In a conventional three-electrode setup, the electrocatalytic activity for the oxygen reduction reaction (ORR) was assessed using a CHI 760E workstation (CHI Instruments, Shanghai, China). Platinum foil served as the counter electrode and Ag/AgCl was employed as the reference electrode. For the preparation of the working electrode, 5 mg of catalyst was dispersed in 1 mL of a Nafion isopropanol solution (comprising 990 μL isopropanol and 10 μL Nafion). The mixture was subjected to ultrasonication for 30 minutes to achieve a homogeneous ink. Subsequently, 20 μL of this catalyst ink was carefully applied to a glassy carbon electrode with a diameter of 5 mm. The same procedure was used to prepare a commercial Pt/C (20 wt%) catalyst solution. Cyclic voltammetry (CV) curves were obtained in a 0.1 M KOH solution saturated with either N_2 or O_2, within a potential range of 0.2 to 0.8 V and at a scan rate of 50 mV s^{-1}. Electrochemical impedance spectroscopy (EIS) measurements were performed with an amplitude of 5 mV over a frequency range of 10,000 to 0.01 Hz. The double-layer capacitance was determined by cyclic voltammograms (CVs) between 1.15 and 1.25 V at different sweep rates in the presence of 0.1 M KOH. The long-term stability of electrocatalysts was investigated by chronoamperometric responses (CA). The rotating ring disk electrode (RRDE) technique was utilized at various rotational speeds ranging from 400 to 2025 rpm with a scan rate of 10 mV s^{-1}. To evaluate long-term stability, Fe_3C@BNC and Pt/C catalysts were tested at a constant voltage of 0.6 V vs. Ag/AgCl in an O_2-saturated electrolyte containing 0.1 M KOH.

The electron transfer number (n) was determined using the Koutecky-Levich equation by analyzing the slope of the best-fit linear line, as follows[2]:

$$\frac{1}{j}=\frac{1}{j_k}+\frac{1}{B\omega^{1/2}} \quad (1)$$

where j, ω, and j_k stand for the measured current, electrode rotation rate and kinetic limiting current, respectively.

The following computation was used to determine the theoretical Levich slope (B):

$$B=0.62nFC_{O_2}D_{O_2}^{2/3}v^{1/6} \quad (2)$$

where n, C_{O_2}, F, v, and D_{O_2} denote the transfer electron number, the oxygen concentration (solution) (1.2×10^{-6} mol cm^{-3}), the Faradaic constant (96485 C mol^{-1}), the kinematic viscosity of the 0.1 M KOH (0.01 cm^2 s^{-1}) and the oxygen diffusion coefficient (1.9×10^{-5} cm^2 s^{-1}).

Additionally, the kinetic properties of the ORR were examined using a rotating RRDE in an O_2-saturated 0.1 M KOH solution with a scan rate of 5 mV s^{-1}. The yield of peroxide species and the number of electrons transferred were determined from the LSV data collected at 1600 rpm using the RRDE, and calculated using the following equations[2]:

$$n=4\times\frac{I_D}{I_D+I_R/N} \quad (3)$$

$$H_2O_2(\%)=200\times\frac{I_R/N}{I_D+I_R/N} \quad (4)$$

The I_D is the disk current and I_R is the ring current, respectively. The N represents the current collection efficiency equaled to 0.37 of the RRDE in our experimental system.

For the oxygen evolution reaction (OER), the polarization curves were recorded in a 1 M KOH solution at a scan rate of 1 mV s^{-1}. The accelerated durability test (ADT) was performed by CV in 1 M KOH solution for 1000 cycles with a scan rate of 100 mV s^{-1}. All electrode potentials were referenced to the reversible hydrogen electrode (RHE) based on the following calculation equations:

$$E_{RHE}=E_{Ag/AgCl}+0.059\times pH+0.197 \quad (5)$$

5. Zn-air battery tests

A Zn-air battery is mainly comprised of three components: the cathode, the anode, and the electrolyte. The preparation of the cathode involves dispersing the catalyst in an aqueous solution, followed by the addition of a Nafion membrane solution to form a homogeneous catalyst slurry with a concentration of 5 mg mL^{-1}. This slurry is then deposited onto carbon paper and allowed to dry, ensuring a catalyst loading of 1 mg cm^{-2} on the carbon paper. For the anode preparation, a zinc sheet is polished with sandpaper to remove any surface oxide layer, and the polished zinc sheet is used as the anode. A mixed solution of 6 M KOH and 0.2 M $Zn(Ac)_2$ serves as the electrolyte. Finally, the cathode, anode, and electrolyte are assembled into a liquid Zn-air battery using a Zn-air battery mold from Changsha Spring Company.

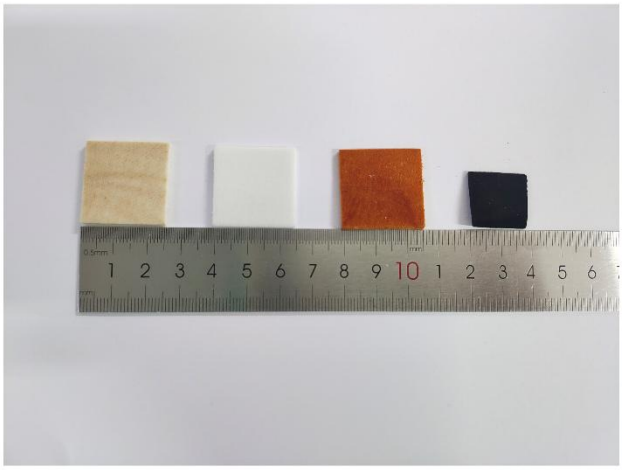

Supplementary Figure 1. Photograph of natural balsa wood, PW, $FeCl_3$-PW, and Fe_3C@BNC.

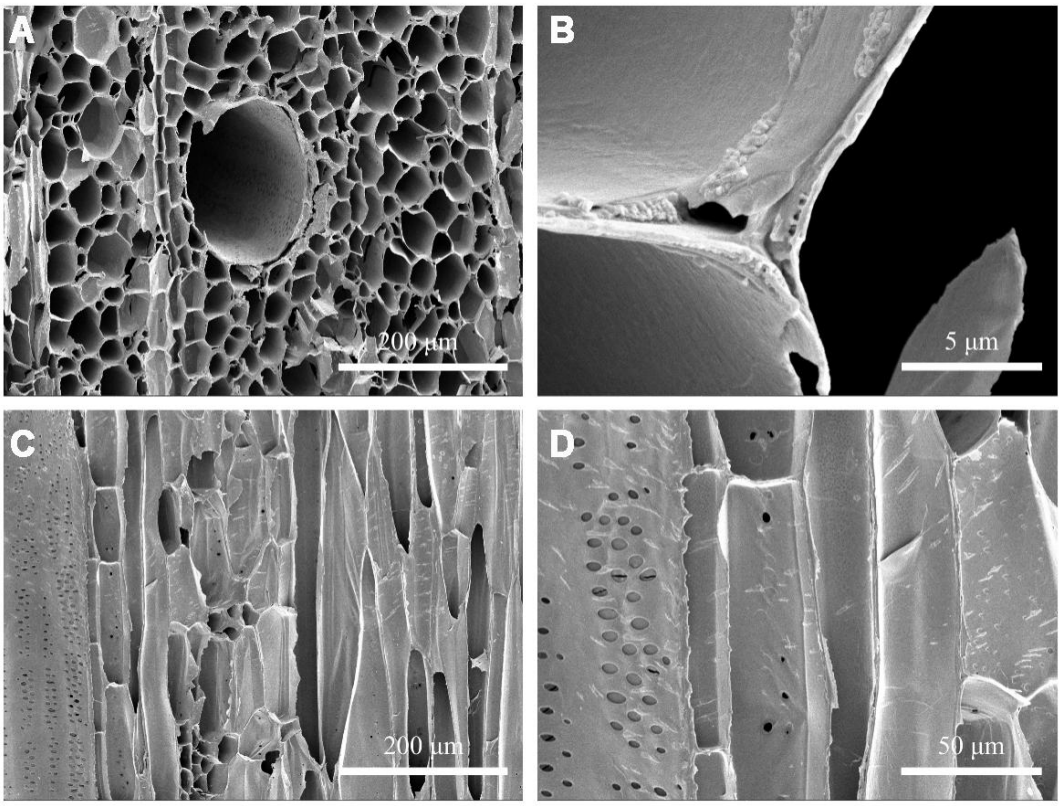

Supplementary Figure 2. (A and B) Top-view and (C and D) side-view SEM images of PW.

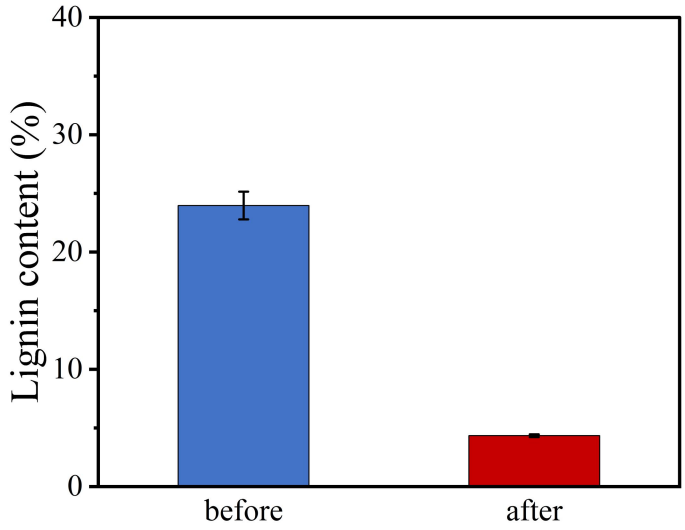

Supplementary Figure 3. Content of lignin in wood before and after reaction (error bars represent mean ± standard deviation, $n = 5$).

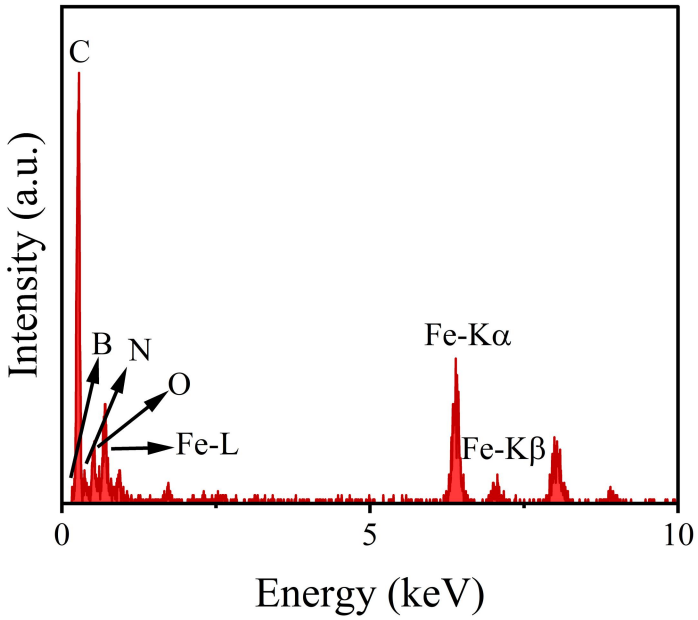

Supplementary Figure 4. EDS spectrum of Fe_3C@BNC.

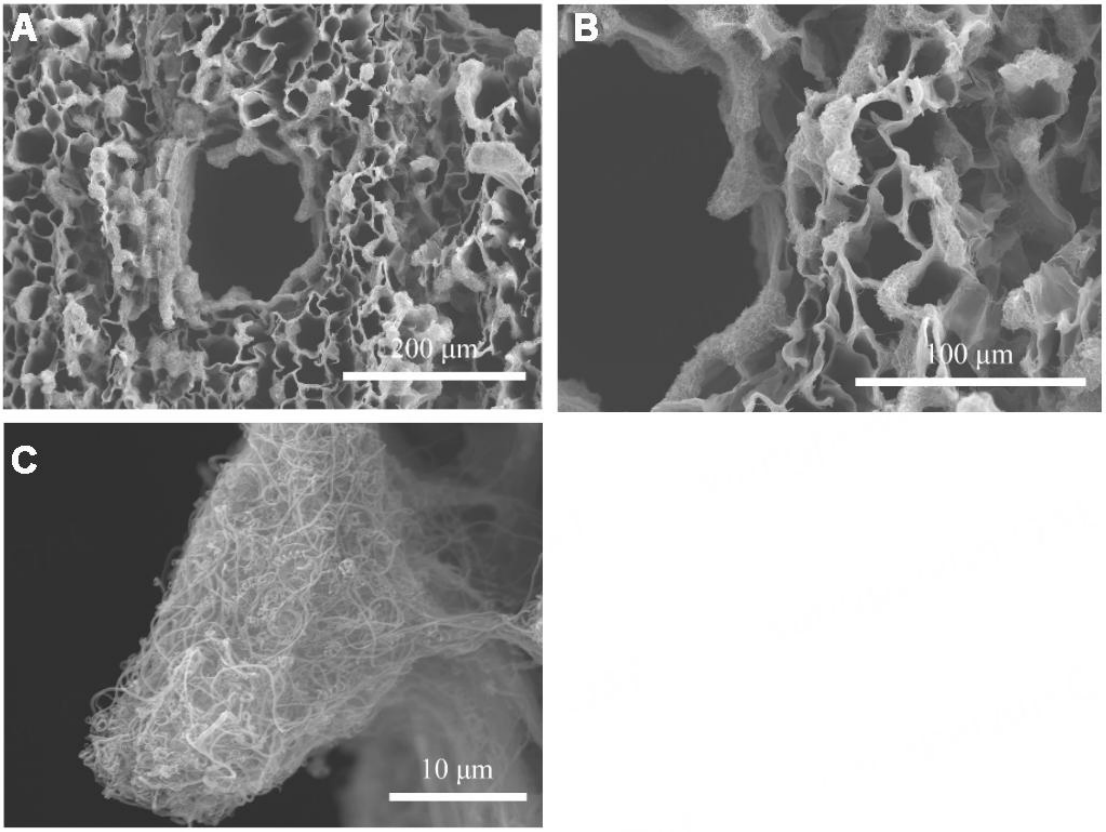

Supplementary Figure 5. Top-view SEM images of Fe_3C@NC.

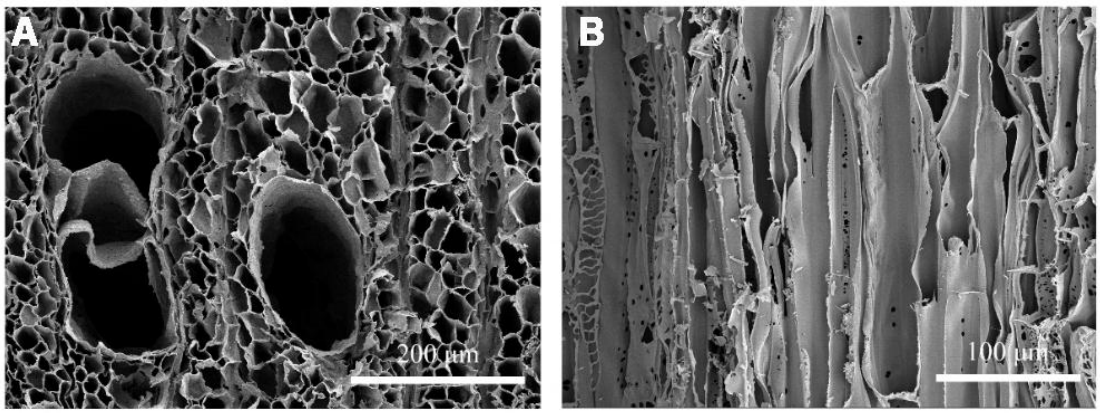

Supplementary Figure 6. (A) Top-view and (B) side-view SEM images of BNC.

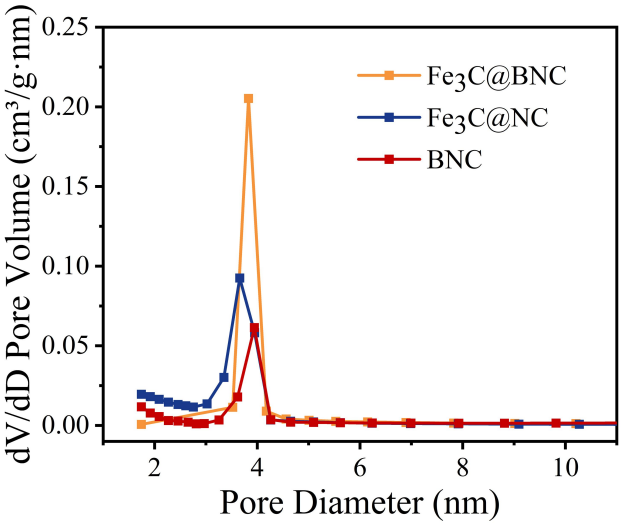

Supplementary Figure 7. Pore size distributions of Fe_3C@BNC, Fe_3C@NC and BNC.

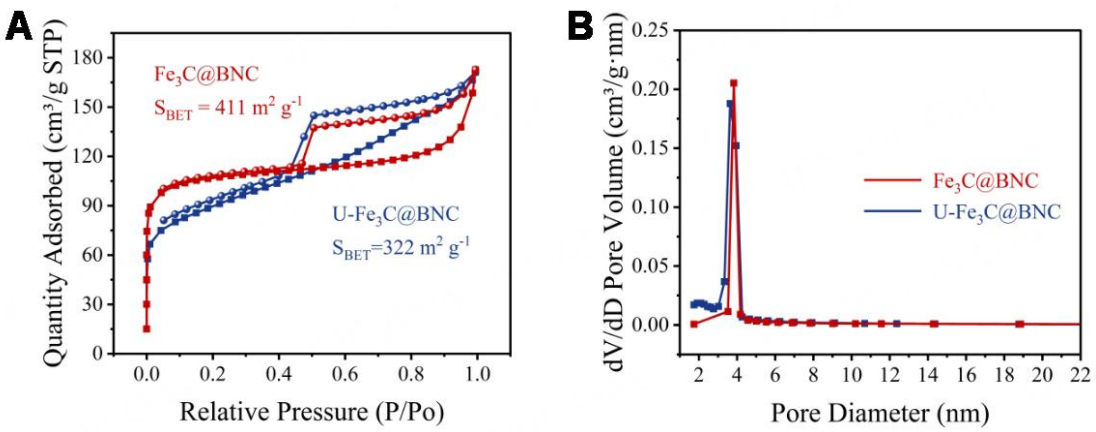

Supplementary Figure 8. N_2 adsorption/desorption isotherms (A) and pore size distributions (B) of Fe_3C@BNC and U-Fe_3C@BNC.

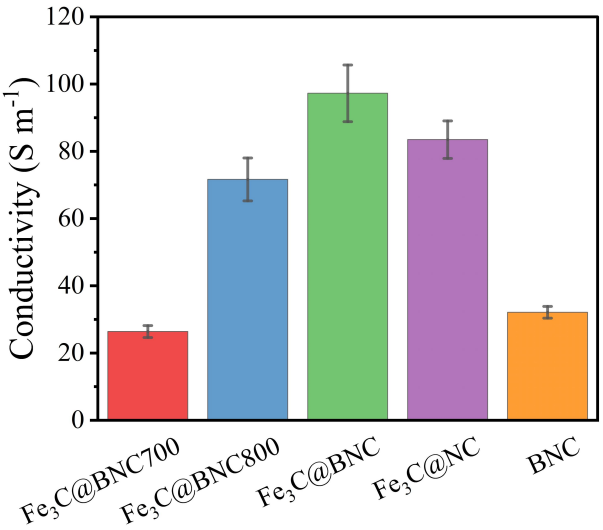

Supplementary Figure 9. Electrical conductivities of BNC, Fe_3C@NC, Fe_3C@BNC and the samples prepared at different pyrolysis temperatures (error bars represent mean ± standard deviation, n = 5).

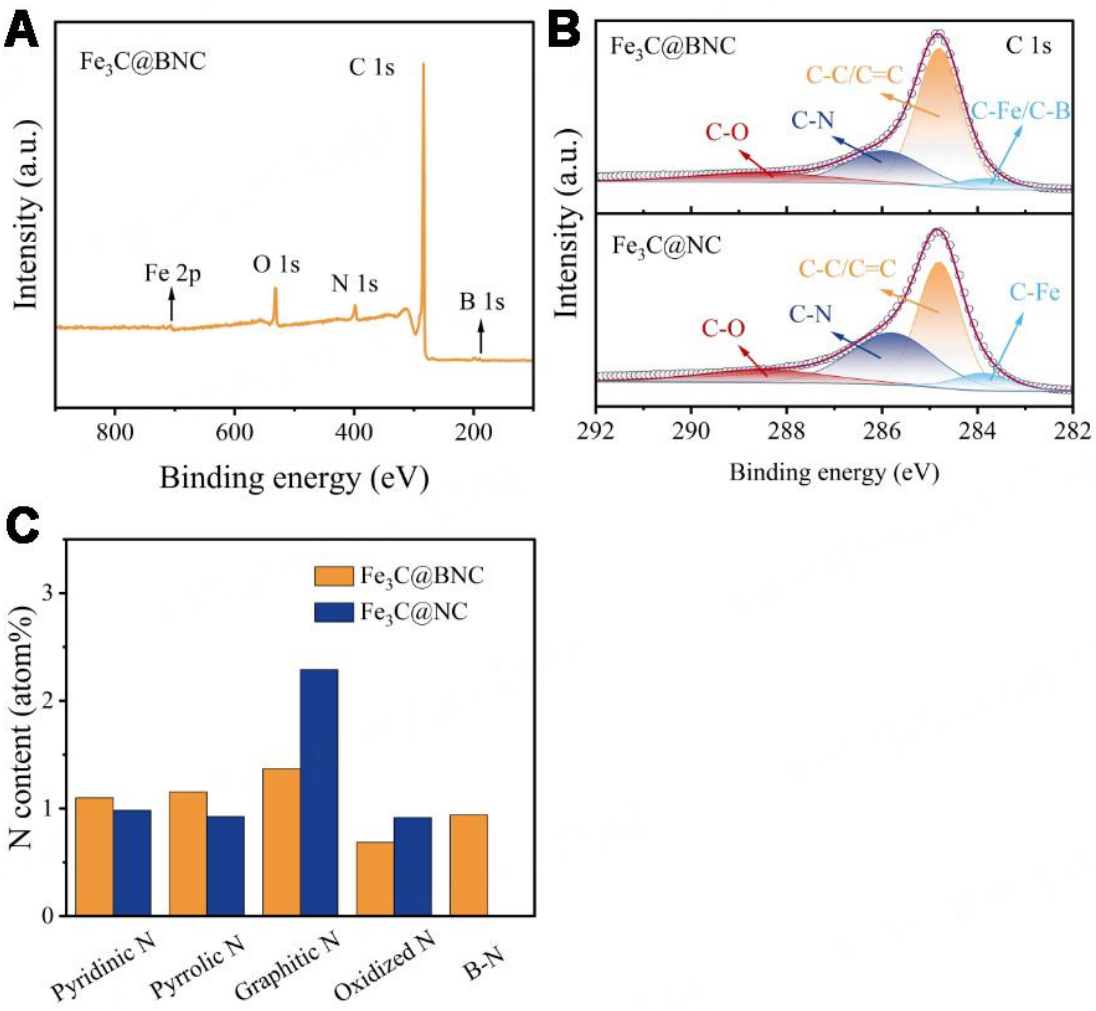

Supplementary Figure 10. (A) XPS survey spectrum of Fe_3C@BNC. (B) High-resolution XPS peak of C 1s. (C) Content of N-doped configuration.

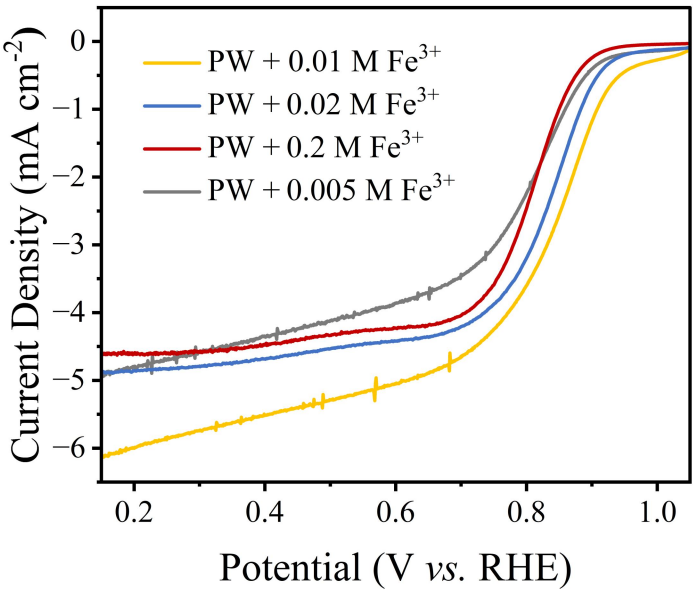

Supplementary Figure 11. LSV curves of electrocatalysts prepared by different Fe^{3+} concentrations in O_2-saturated 0.1 M KOH at 1600 rpm with a scan rate of 5 mV s^{-1}.

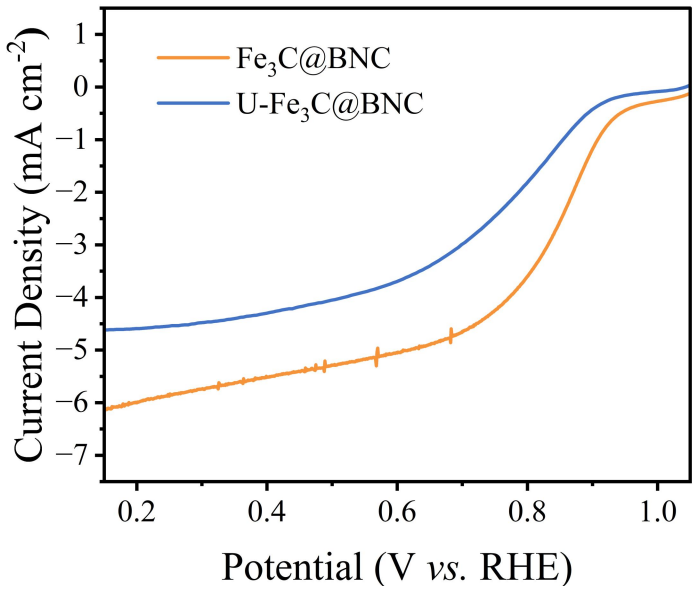

Supplementary Figure 12. LSV curves of Fe_3C@BNC and U-Fe_3C@BNC in O_2-saturated 0.1 M KOH at 1600 rpm with a scan rate of 5 mV s^{-1}.

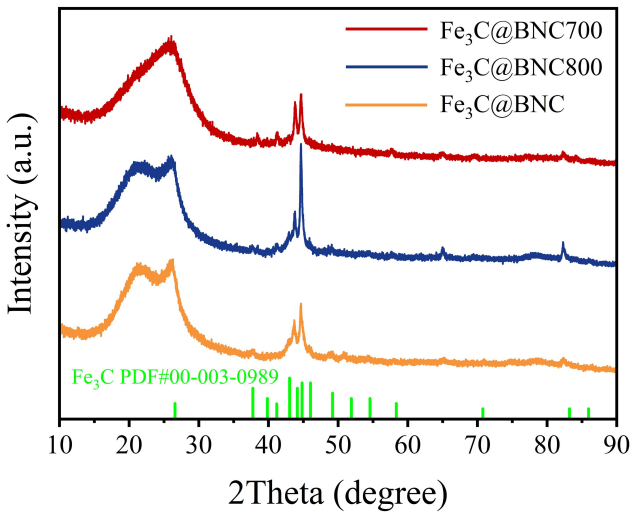

Supplementary Figure 13. The XRD patterns of Fe_3C@BNC prepared at different pyrolysis temperatures.

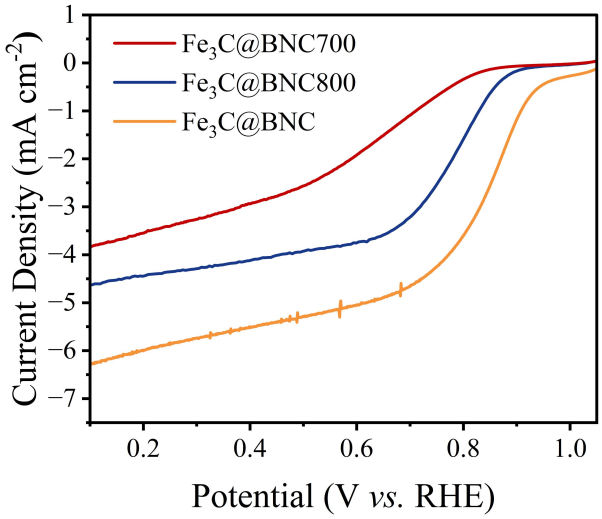

Supplementary Figure 14. LSV curves of Fe_3C@BNC prepared at different pyrolysis temperatures in O_2-saturated 0.1 M KOH at 1600 rpm with a scan rate of 5 mV s^{-1}.

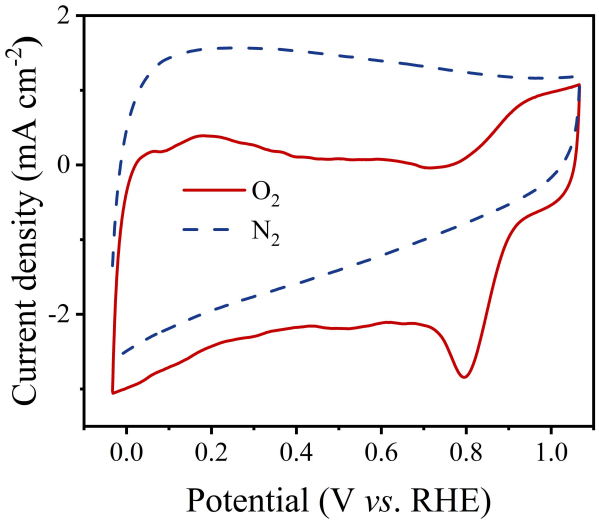

Supplementary Figure 15. CV curves of the Fe_3C@BNC electrocatalyst collected in N_2- and O_2-saturated 0.1 M KOH electrolyte.

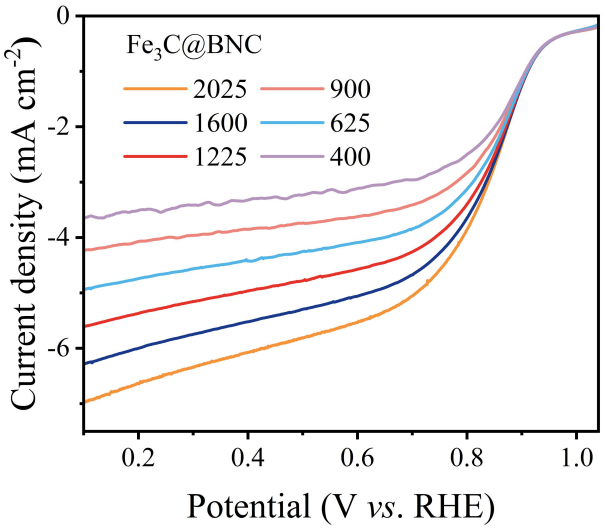

Supplementary Figure 16. The LSV curves of Fe_3C@BNC with various rotating rates.

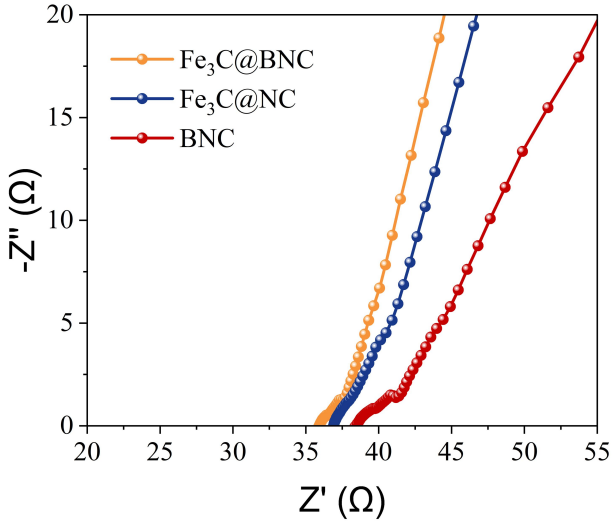

Supplementary Figure 17. Nyquist plots of Fe_3C@BNC, Fe_3C@NC and BNC at O_2-saturated 0.1 M KOH electrolyte.

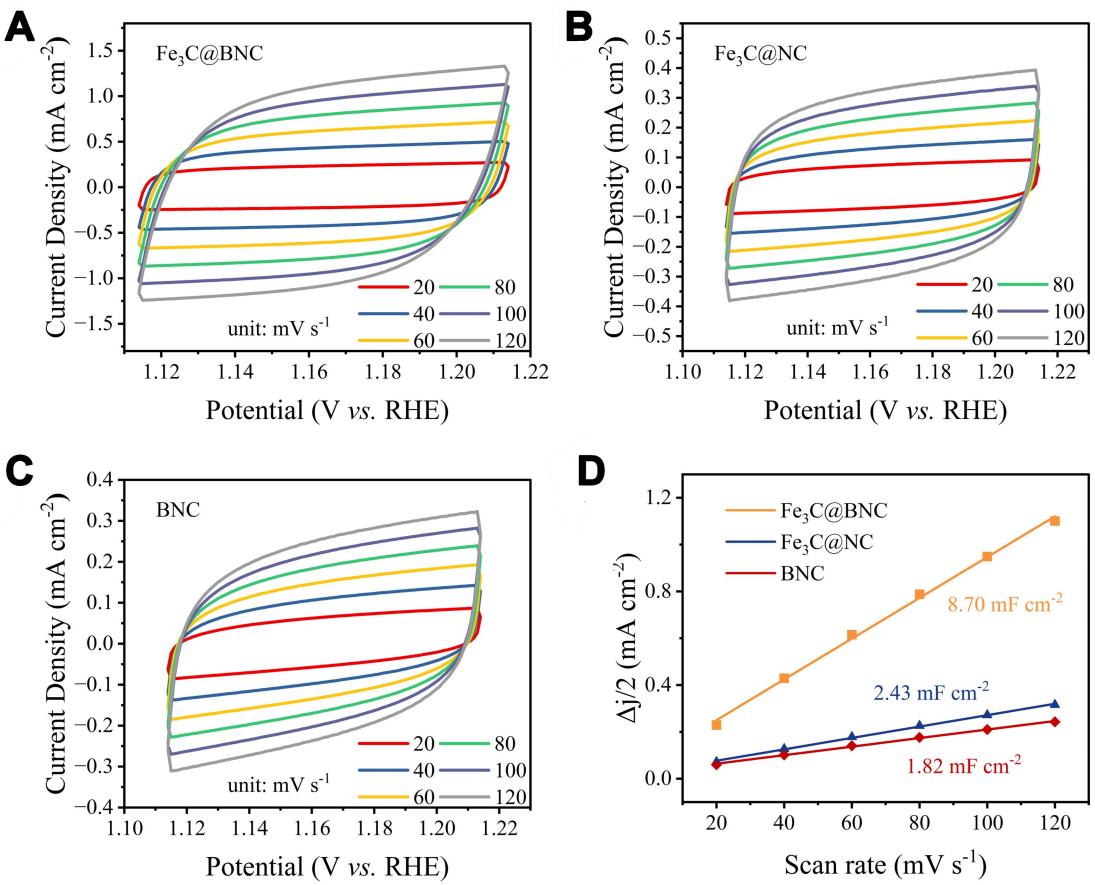

Supplementary Figure 18. CV curves of (A) Fe_3C@BNC, (B) Fe_3C@NC and (C) BNC at various scan rates from 20 to 120 mV s^{-1}. (D) The summarized double layer capacitance (Cdl) of Fe_3C@BNC, Fe_3C@NC, and BNC.

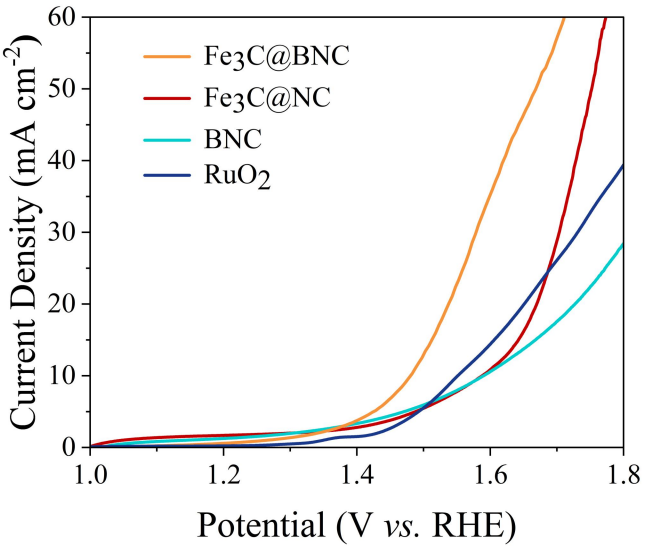

Supplementary Figure 19. OER LSV curves of Fe_3C@BNC, Fe_3C@NC, BNC, and RuO_2 in 0.1 M KOH electrolyte.

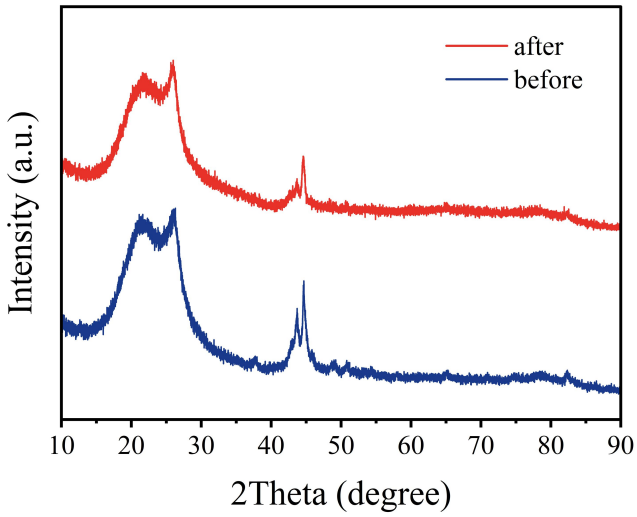

Supplementary Figure 20. The XRD patterns of Fe_3C@BNC before and after 1000 cycles CV test.

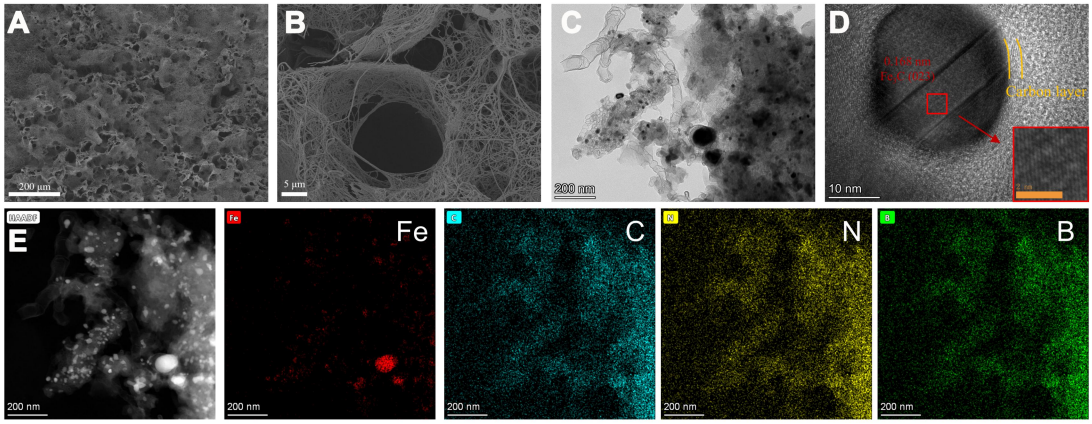

Supplementary Figure 21. SEM (A and B) and TEM (C and D) images of Fe_3C@BNC image; and EDS mapping (E) of different elements in Fe_3C@BNC.

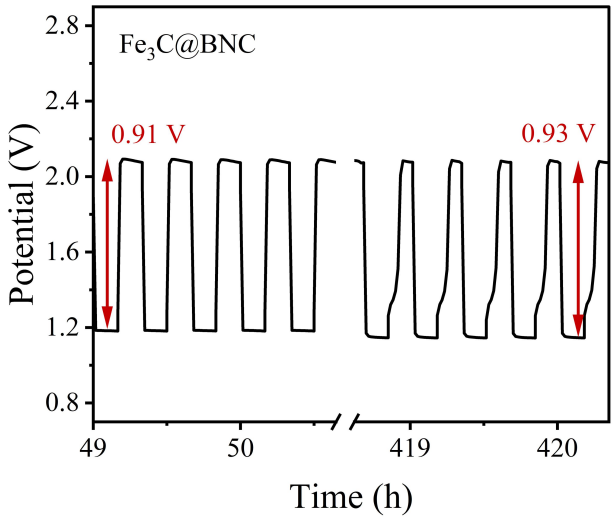

Supplementary Figure 22. Galvanostatic discharge/charge curves of Fe_3C@BNC at 49~50 h and 419~420 h, respectively.

Supplementary Table 1. Comparison of N and B atomic % content in Fe_3C@BNC and Fe_3C@NC

	N atomic %	B atomic %
Fe_3C@BNC	5.25	1.13
Fe_3C@NC	5.11	/

The N and B contents were determined by XPS analysis.

Supplementary Table 2. EIS data of the three samples

Samples	Fe_3C@BNC	Fe_3C@NC	BNC
Rp	35.9	36.9	38.5

Supplementary Table 3. Activity comparison of wood-derived carbon-based catalysts toward oxygen electrocatalysis

Catalyst	$E_{1/2}$ (V vs. RHE)	$E_{j=10}$ (V vs. RHE)	ΔE ($E_{j=10}-E_{1/2}$) (V)	Ref.
Fe_x/FeN_3S_1-C	0.9	1.548	0.65	[3]
SAC-FeN-WPC	0.85	1.64	0.79	[4]
Co@NCW	0.89	1.64	0.75	[5]
Co@D-NCNT/CW	0.84	1.48	0.64	[6]
Co/CoO@NWC	0.85	1.62	0.77	[7]
CoFe@NC/WC-850	0.80	1.545	0.75	[8]
Fe_3C@BNC	0.83	1.48	0.65	This work

Reference

1. Sluiter A, Hames B, Ruiz R O, Scarlata C, Sluiter J, Templeton D. Determination of structural carbohydrates and lignin in biomass. *Biomass Anal Technol Team Lab Anal Proced*. 2004;2011:1-14.

2. Huo L, Lv M, Li M, et al. Amorphous MnO_2 lamellae encapsulated covalent triazine polymer-derived multi-heteroatoms-doped carbon for ORR/OER bifunctional electrocatalysis. *Adv. Mater*. 2024;36:2312868.

3. Chen J, Qiu C, Zhang L, et al. Wood-derived Fe cluster-reinforced asymmetric single-atom catalysts and weather-resistant organohydrogel for wide-temperature flexible Zn-air batteries. *Energy. Environ. Sci*. 2024;17:4746-57.

4. Zhong L, Jiang C, Zheng M, et al. Wood carbon based single-atom catalyst for rechargeable Zn–air batteries. *ACS. Energy. Lett.* 2021;6:3624-33.

5. Li W, Wang F, Zhang Z, Min S. Graphitic carbon layer-encapsulated Co nanoparticles embedded on porous carbonized wood as a self-supported chainmail oxygen electrode for rechargeable Zn-air batteries. *Appl. Catal. B.* 2022;317:121758.

6. Chen Z, Chen H, Li T, et al. Defective wood-based chainmail electrocatalysts boost performances of seawater-medium Zn-air batteries. *J. Energy. Chem.* 2025;102:134-43.

7. Cui X, Liu Y, Han G, et al. Wood-derived integral air electrode for enhanced interfacial electrocatalysis in rechargeable zinc-air battery. *Small.* 2021;17:2101607.

8. Ao K, Zhang X, Nazmutdinov RR, et al. Hierarchical CoFe@N-doped carbon decorated wood carbon as bifunctional cathode in wearable Zn-air battery. *Energy. Environ. Mater.* 2023;7:e12499.